Journal of Alloys and Compounds 509 (2011) 6781–6786

Contents lists available at ScienceDirect

Journal of Alloys and Compounds

journal homepage: www.elsevier.com/locate/jallcom

Kinetics of nanoscale precipitation in Ni–Fe–Al alloys: A magnetic monitoring approach

Nagehan Duman*, Amdulla O. Mekhrabov, M. Vedat Akdeniz

Department of Metallurgical and Materials Engineering, Middle East Technical University, TR-06531 Ankara, Turkey

ARTICLE INFO

Article history:
Received 21 February 2011
Received in revised form 25 March 2011
Accepted 30 March 2011
Available online 5 April 2011

Keywords:
Intermetallics
Nickel aluminide
Precipitation
Kinetics
Magnetic measurements

ABSTRACT

In this study, time–temperature dependence and kinetic aspects of nanoscale precipitation responsible for strengthening of $Ni_{50}Fe_xAl_{50-x}$ alloys with $x = 20$, 25 and 30 were investigated by temperature-scan and isothermal magnetic measurements in a vibrating sample magnetometer. Temperature-scan magnetization curves contained a magnetization rise for all studied alloys at temperatures above the Curie transition of the primary phase. These transient rises at relatively higher temperatures were associated with the formation of secondary ferromagnetic precipitates, identified as nano-sized body centered cubic α crystallites by microstructural observations under the transmission electron microscope. The isothermal kinetics of ferromagnetic α-phase precipitation was analyzed with the Johnson–Mehl–Avrami model. The Avrami exponent was determined to be close to unity and independent of the extent of precipitation, annealing temperature and alloy composition. It was concluded that α-phase precipitation was governed by a diffusion controlled growth process with decreasing growth rate, which closely resembles continuous precipitation kinetics. The activation energies, ranging between 75 and 83 kJ/mol, were utilized to construct magnetically assessed isothermal transformation diagrams of precipitation. Conforming to the kinetic analysis, annealing at an intermediate temperature ensures precipitation of fine second phase particles and brings about a significant hardening effect, whereas a higher annealing temperature yields coarser precipitates and a smaller extent of precipitation hardening.

1. Introduction

Nickel–aluminum (NiAl) is one of the most promising intermetallic compounds that have been extensively studied for high temperature structural applications [1–3]. In addition to its high melting point and low density, the ordered NiAl alloy exhibits excellent corrosion and oxidation resistance. On the other hand, the improvement of room temperature ductility and high temperature strength requires further attention for utilization in demanding applications. In this respect, the incorporation of Fe into the NiAl system has been shown to remarkably modify the structural properties [4–6] and promote precipitation of a fine body centered cubic (BCC) α-phase, which strengthens the alloy [7–9]. Although the α-precipitates are softer than the BCC β-matrix, they induce changes in the slip system and strengthen the alloys via precipitation hardening through a dislocation pinning effect [7,10].

From a general point of view, while very fine precipitates provide the largest strengthening effect, a balance between strength and ductility can be attained with relatively coarser precipitates. However, for long-term applications, evolution of α precipitates at high temperatures should be clarified in order to determine an upper limit where the microstructure coarsens resulting in reduced strength. A convenient annealing heat treatment is also essential to form desirable precipitates. Therefore, in addition to its temperature dependence, kinetic aspects and mechanism of nanoscale α-phase precipitation in Ni–Fe–Al alloys have attracted considerable interest [11,12]. However, determination of time and temperature dependent changes in these nanoscale precipitates using high-resolution electron microscopy is quite laborious and requires extensive image analysis [11].

In a few studies, magnetic monitoring approach was implemented to replace conventional thermal analysis as a tool to successfully reveal crystallization kinetics in amorphous-matrix nanocrystalline alloys. For instance, Luborsky [13] attempted to model the time and temperature dependent changes in magnetic parameters such as coercivity and anisotropy with the Johnson–Mehl–Avrami equation. Later, this approach was used to understand crystallization in Ni–P precursor films from the amorphous state [14]. Recently, using similar magnetic monitoring approaches, the disproportionation reaction observed in cast rare-earth transition metal alloys [15,16] and crystallization kinetics of Fe-based soft magnetic amorphous alloys were examined

* Corresponding author at: Department of Metallurgical and Materials Engineering, NOVALAB, Middle East Technical University, TR-06531 Ankara, Turkey.
Tel.: +90 312 210 2534; fax: +90 312 210 2518.
E-mail address: nduman@metu.edu.tr (N. Duman).

0925-8388/$ – see front matter © 2011 Elsevier B.V. All rights reserved.
doi:10.1016/j.jallcom.2011.03.167

[17]. To the best of our knowledge, kinetics of such precipitation reactions occurring at the nanoscale has not been examined via magnetic measurements for intermetallic alloys. Therefore, this study will be the first to discuss the kinetic aspects of α-phase precipitation in $Ni_{50}Fe_xAl_{50-x}$ (x = 20, 25, and 30) alloys by utilizing a non-conventional characterization technique which exploits the ferromagnetic character of the precipitating phase [18]. In the current work, precipitation was monitored by magnetization measurements encompassing both temperature-scan and isothermal experiments with a vibrating sample magnetometer. Transmission electron microscopy (TEM) and micro-hardness measurements were conducted to support the kinetic analysis.

2. Experimental procedure

The $Ni_{50}Fe_xAl_{50-x}$ alloys with x = 20, 25 and 30 were prepared by arc-melting of high purity 99.9% Ni, Fe and Al elements under argon atmosphere. Ingots were re-melted for four times to ensure compositional homogeneity.

The kinetics of precipitation was studied using a vibrating sample magnetometer (VSM, ADE Magnetics EV9). Temperature-scan measurements were done under 500 Oe applied field from room temperature to 973 K at a scan rate of 5 K/min whereas isothermal magnetization experiments were carried out at various temperatures ranging from 750 to 950 K with 25 K increments. Magnetization was measured every 5 K during temperature-scan experiments and every 3 min during isothermal annealing.

Vickers micro-hardness measurements (Hv 0.025) were performed phase-selectively on as-cast and annealed samples by an automated micro-hardness tester (Shimadzu HMV-2). Averages of at least eight indentations were reported as the micro-hardness values.

A field-emission high-resolution transmission electron microscope (JEOL JEM 2100F) was used to examine the precipitates at an acceleration voltage of 200 kV. The alloys for TEM study were prepared by an annealing treatment at 673 K and 873 K for 168 h, followed by air cooling to room temperature. Disc shaped foils of 3 mm diameter were twin-jet electropolished (Fischione Instruments Model 110) in a solution of 10% perchloric acid rest methanol at a temperature of −55 °C and an applied voltage of 11 V. Samples were plasma-cleaned (Fischione Model 1020) prior to TEM investigations.

3. Results and discussion

The study of kinetics in solid state processes such as phase transformations, crystallization or crystal-growth and precipitation reactions often utilizes well-known Johnson–Mehl–Avrami (JMA) equation. Provided that the kinetic process of precipitation obeys the JMA relation, time exponent (n) and activation energy (E_a) for the precipitation reaction can be found.

In addition, measured values of time dependent magnetization under an applied magnetic field (e.g. 500 Oe is applied in this study) can be implemented in JMA model by relating the fraction transformed (α_t) to magnetization at any time during annealing (M_t), initial magnetization (M_i) and final magnetization (M_f) in the form $\alpha_t = (M_t - M_i)/(M_f - M_i)$. An important point to note in this approach is the method used to estimate the final magnetization. The experimentally obtained time dependent magnetization was first least-squares fit to an exponential rise function and then extrapolated to a sufficiently long time (~8 h). By this means, the maximum attainable fraction of precipitates, taken as $\alpha_t = 1$, was assumed to be reached at such long isothermal holding times, as illustrated in Fig. 1.

The magnetization behavior of $Ni_{50}Al_{50-x}Fe_x$ alloys (x = 20, 25 and 30) was examined by continuous heating scans in VSM. Alloys undergo Curie transition below 500 K, and above these transition temperatures, magnetization values begin to rise again starting at around 700 K (Fig. 2). This is associated with the precipitation of a secondary ferromagnetic phase with a higher Curie transition compared to the primary β-phase. Relevant phase diagrams [8,19,20] support that this ferromagnetic phase is an Fe-rich BCC phase formed within the miscibility gap between ordered (B2, β-phase) and disordered (α-Fe) BCC phases.

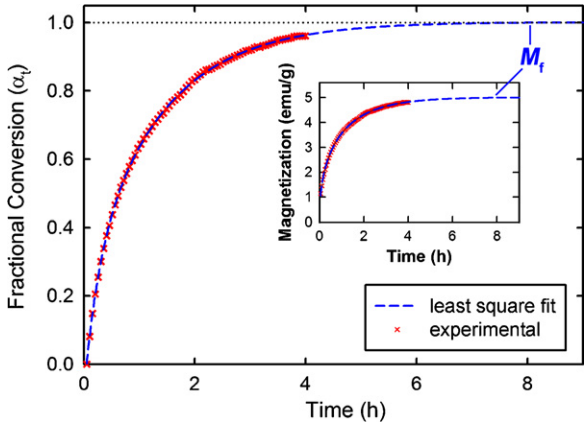

Fig. 1. An example illustrating the estimation procedure of maximum magnetization (M_f) values using experimentally determined time-dependent magnetization in VSM.

In order to study the temperature dependence and kinetics of precipitation of the mentioned ferromagnetic phase, isothermal magnetization measurements were carried out at several selected temperatures marked in Fig. 2 over the temperature range where transient rises in magnetization are seen. Isothermal kinetics treatment of the magnetization data covers temperatures above 800 K since lower temperatures do not provide practical rates of magnetization.

Fig. 3 shows the time-dependent magnetization behaviors of alloys measured over a temperature range of 800–900 K in 25 K intervals under an applied field of 500 Oe for a duration of 2 h. Magnetization increases gradually with a decreasing rate with time in all isothermal magnetization experiments. Since an increase in the isothermal temperature results in increased magnetization and rate of magnetization with respect to time, it is clear that precipitation, as monitored by magnetization, is a thermally activated process favored at higher annealing temperatures.

It is also seen in Fig. 3 that non-zero magnetization values are recorded for the very first measurements following the relatively fast heating stage (50 K/min) up to the isothermal temperature. Thus, it could be stated that precipitation as monitored by isothermal magnetization does not show an apparent incubation period. This behavior was previously encountered in studies utilizing a similar magnetic monitoring approach and was attributed to the fact that incubation takes place during the heat-up stage obscuring its observation [15].

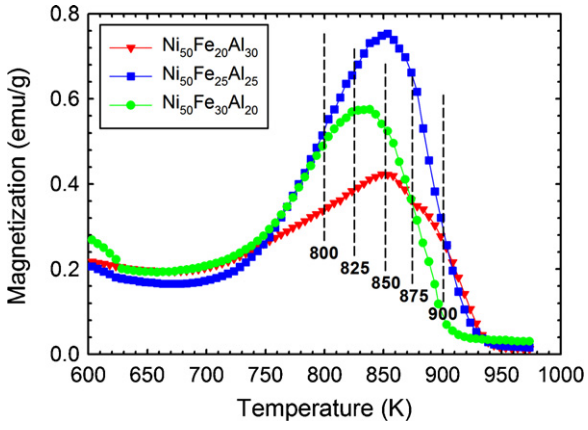

Fig. 2. Thermomagnetization curves of alloys above 600 K where the temperatures for isothermal magnetization measurements are marked.

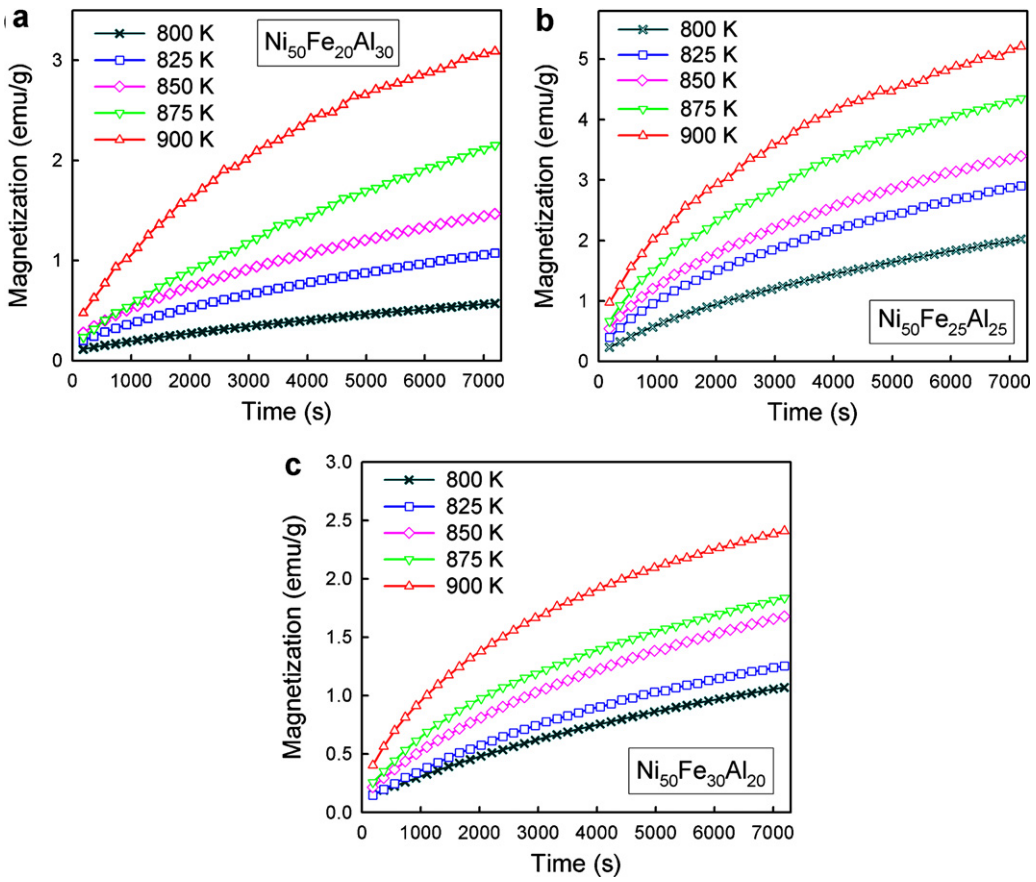

Fig. 3. Time-dependent magnetization curves of (a) $Ni_{50}Fe_{20}Al_{30}$, (b) $Ni_{50}Fe_{25}Al_{25}$ and (c) $Ni_{50}Fe_{30}Al_{20}$ alloys between 800 K and 900 K with 25 K increments.

Fig. 4 shows the time and temperature dependence of magnetization rates during isothermal measurements in VSM. Increase in the isothermal temperature above 750 K results in sharp rises in magnetization rates, particularly for the early stages of precipitation (10 min curve), which is indicative of notable precipitate growth rates. However, below 750 K magnetization increments are marginal at all measurement times (10, 30 and 120 min curves). Therefore, by choosing an appropriate annealing temperature such as 673 K, one could form desirable fine precipitates that would impart an ultimate strengthening effect. On the other hand, following an annealing heat treatment where notable growth rates are encountered (873 K in this case), significant losses in precipitation strengthening are foreseeable.

Annealing at 673 K promotes the formation of fine α-Fe precipitates within the β-phase matrix that impose significant hardening

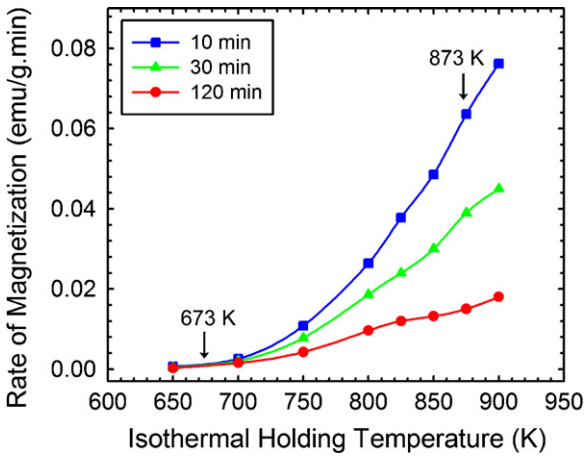

Fig. 4. Rate of magnetization at different measurement times as a function of temperature in isothermal VSM experiments. The curves correspond to the $Ni_{50}Fe_{25}Al_{25}$ alloy.

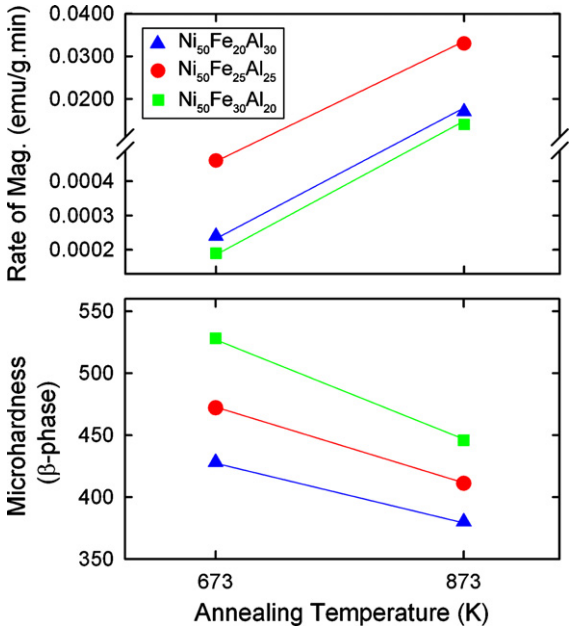

Fig. 5. Correlation between average rates of magnetization and micro-hardness of the primary β-phase.

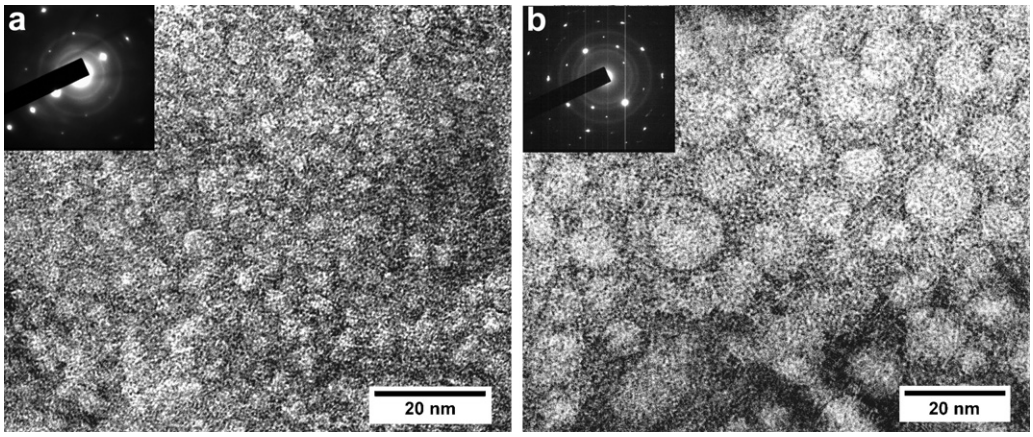

Fig. 6. Bright field TEM micrographs and corresponding selected area diffraction patterns of $Ni_{50}Fe_{25}Al_{25}$ alloy at annealed (a) 673 K, and (b) 873 K.

(20–55% gain in hardness relative to as-cast samples) via dislocation pinning. It can be stated that these precipitates attained their optimum size because an increase in the annealing temperature to 873 K caused drops in hardness by ~10–15%. This could be related with the coarser microstructure formed at high temperatures [7] in accordance with the significant increases in rates of magnetization during isothermal scans at such high temperatures in VSM. In this respect, it is clear from Fig. 5 that an increase in the average rate of magnetization causes decreased micro-hardness of the primary β-phase within which ferromagnetic precipitates are formed.

In our previous study [12], solidification microstructures of as-cast $Ni_{50}Fe_xAl_{50-x}$ alloys with $x = 20$, 25 and 30 were studied. The $Ni_{50}Fe_{20}Al_{30}$ alloy revealed coarse grains of a single B2 type β-phase, whereas $Ni_{50}Fe_{25}Al_{25}$ and $Ni_{50}Fe_{30}Al_{20}$ contained typical off-eutectic microstructure consisting of proeutectic B2 type β-dendrites and interdendritic eutectic (β and γ phases). Fig. 6 shows the TEM microstructures and selected area diffraction patterns of the dendritic regions in $Ni_{50}Fe_{25}Al_{25}$ alloy. The high-density fine BCC α-phase precipitates appear as bright regions in the size range of 3–5 nm distributed uniformly within the matrix of the alloy annealed at 673 K (Fig. 6a). In conformity with reduced hardness and remarkable growth rates deduced from large average rate of magnetization at 873 K isotherm (Fig. 5), the microstructure of the alloy annealed at this temperature

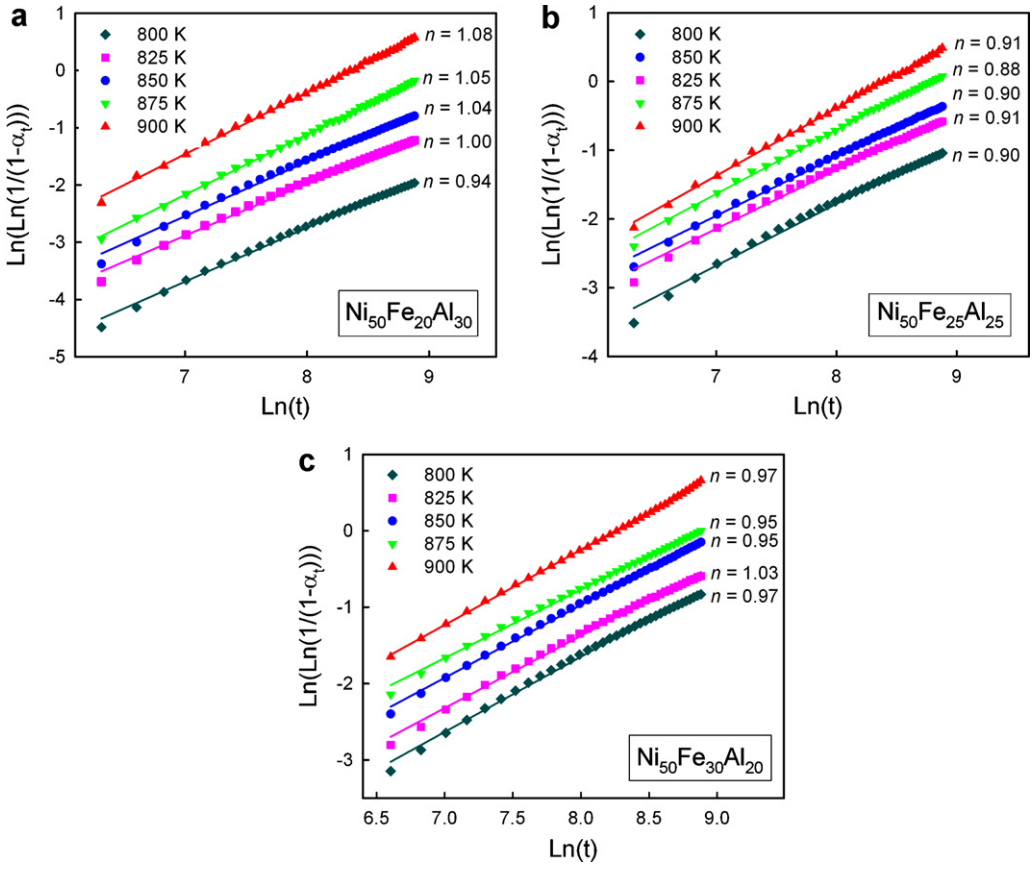

Fig. 7. Avrami plots for (a) $Ni_{50}Fe_{20}Al_{30}$, (b) $Ni_{50}Fe_{25}Al_{25}$ and (c) $Ni_{50}Fe_{30}Al_{20}$ alloys.

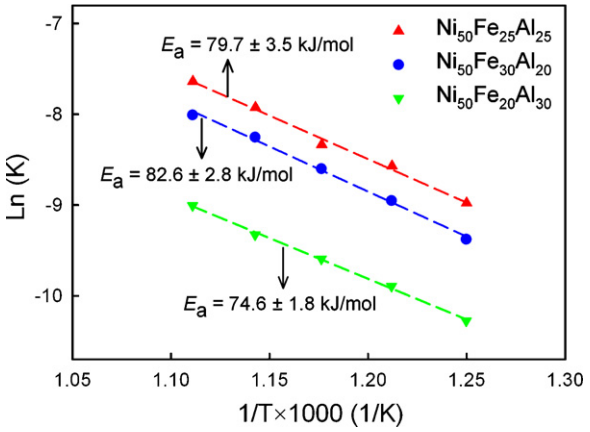

Fig. 8. Activation energies of precipitation as monitored by magnetization measurements.

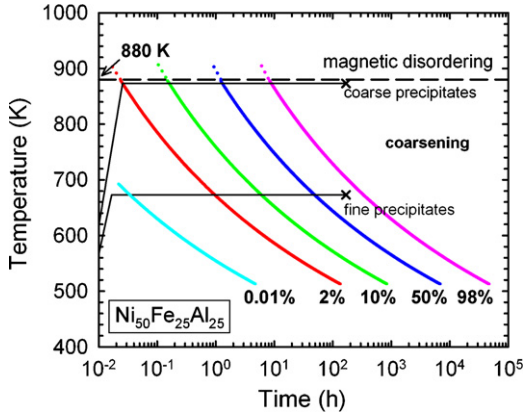

Fig. 9. Magnetically assessed time–temperature dependence of α-phase precipitation in the $Ni_{50}Fe_{25}Al_{25}$ alloy.

is coarser and precipitate sizes lie in the range of 8–15 nm (Fig. 6b).

Fig. 7 shows the Avrami plots drawn for various annealing temperatures. The Avrami time exponent for the entire range of alloys are close to $n = 1$, indicating that the precipitation reaction follows a first order kinetics. Therefore, it can be stated that the investigated process is predominated by diffusion controlled growth [21]. The straight line fits do not significantly deviate for the whole timescale of the measurements which means that precipitation occurs without a change in its mechanism throughout the entire process.

Activation energies (E_a) for the growth process were determined in Fig. 8 employing isothermal magnetization measurements at several temperatures where the ferromagnetic phase precipitates. The activation energies were found to range between 74.6 kJ/mol and 82.6 kJ/mol with a maximal deviation of ±3.5 kJ/mol. The slight differences in calculated activation energies for studied alloys might be related to variation in the composition of the primary β-phase where α crystallites precipitate.

The low activation energies together with non-zero magnetizations at the beginning of isothermal measurements (no detectable incubation time) can indicate a process dominated by the growth of already existing nuclei. Considering diffusivities in ternary Ni–Al–Fe alloys, the relatively lower activation energies deduced here might also be related to compositional effects on diffusivity and influence of thermal vacancies [22].

Having found the magnetically assessed kinetic parameters (E_a, n and K), the general precipitation behavior of nano-sized BCC α-phase can be followed by plotting the isothermal transformation diagram provided in Fig. 9. The magnetic monitoring approach is limited by the magnetic disordering temperature above which the magnetization of alloys cease and the growth process cannot be magnetically tracked. These upper limits were taken as the maxima of the derivative of temperature-scan magnetization curves (Fig. 2). Actually, during isothermal experiments, temperatures above magnetic disordering yielded lower rates of magnetization and suppressed magnetization values. The reason why the overall process cannot be magnetically monitored above a certain temperature could be the competition between the diffusion controlled precipitation process and the magnetic disordering induced in the ferromagnetic α-phase at high temperatures.

The diffusion controlled growth of precipitates is highly dependent on annealing temperature and proceeds faster at a higher temperature. The completion of transformation, i.e. $\alpha \sim 1$, is referred as the state where the equilibrium fraction of α-phase precipitates is reached. For instance, transformation will be completed at 873 K within 10 h for $Ni_{50}Fe_{20}Al_{30}$ and $Ni_{50}Fe_{25}Al_{25}$ alloys, and 6 h for the $Ni_{50}Fe_{30}Al_{20}$ alloy, and further annealing will cause the microstructure to become unstable and coarsen to a lower density of larger particles. On the other hand, at a lower annealing temperature (e.g. 673 K), transformation is almost complete in 168 h ($\alpha \approx 0.97$, 0.90, and 0.97 for $Ni_{50}Fe_{20}Al_{30}$, $Ni_{50}Fe_{25}Al_{25}$ and $Ni_{50}Fe_{30}Al_{20}$, respectively) yielding finer precipitates without further coarsening.

4. Conclusions

In this study, time–temperature dependence and kinetic aspects of α-phase precipitation in $Ni_{50}Fe_xAl_{50-x}$ alloys for $x = 20$, 25, 30 were investigated by continuous heating and isothermal experiments in vibrating sample magnetometer. The α-phase precipitation process was treated by the JMA kinetic model where the time exponent for the process assumed values around $n = 1$, independent of the extent of precipitation, utilized isothermal temperature and alloy composition. The activation energies for the precipitation in three different alloy compositions were determined to range between 75 and 83 kJ/mol. It is concluded that the examined process is diffusion controlled growth with decreasing growth rate. Corresponding isothermal transformation diagrams, providing a general picture for the nano-sized BCC α-phase precipitation, were drawn by using magnetically assessed kinetic parameters.

Depending on the measured rates of magnetization at utilized temperatures in isothermal runs, remarkable precipitate growth rates are expected at annealing temperatures higher than around 750 K. It is intriguing that alloys annealed at 673 K presented a microstructure comprising of fine precipitates which provided ultimate hardening of the matrix involving precipitates, in accordance with magnetic measurements. As opposed to that, a higher annealing temperature of 873 K resulted in a coarser microstructure accompanied by a corresponding reduction in the extent of precipitation hardening.

Acknowledgement

One of the authors (N.D.) acknowledges OYP Program at Middle East Technical University for financially supporting the graduate study.

References

[1] D.B. Miracle, Acta Metall. Mater. 41 (1993) 649–684.
[2] J.A. Jimenez, S. Klaus, M. Carsi, O.A. Ruano, G. Frommeyer, Acta Mater. 47 (1999) 3655–3662.
[3] B. Zeumert, G. Sauthoff, Intermetallics 5 (1997) 563–577.

[4] E.P. George, C.T. Liu, J.A. Horton, C.J. Sparks, M. Kao, H. Kunsmann, T. King, Mater. Charact. 39 (1997) 665–686.
[5] A. Inoue, T. Masumoto, H. Tomioka, J. Mater. Sci. 19 (1984) 3097–3106.
[6] R. Kainuma, S. Imano, H. Ohtani, K. Ishida, Intermetallics 4 (1996) 37–45.
[7] S. Guha, I. Baker, P.R. Munroe, J.R. Michael, Mater. Sci. Eng. A 152 (1992) 258–263.
[8] S.M. Hao, T. Takayama, K. Ishida, T. Nishizawa, Metall. Trans. A 15 (1984) 1819–1828.
[9] P.R. Munroe, M. George, I. Baker, F.E. Kennedy, Mater. Sci. Eng. A 325 (2002) 1–8.
[10] A. Misra, R. Gibala, Metall. Mater. Trans. A 28 (1997) 795–807.
[11] M. Muñoz-Morris, N. Calderon, D. Morris, J. Mater. Sci. 43 (2008) 3674–3682.
[12] N. Duman, A.O. Mekhrabov, M.V. Akdeniz, Mater. Charact., in press, doi:10.1016/j.matchar.2011.04.006.
[13] F.E. Luborsky, J. Appl. Phys. 57 (1985) 3592–3594.
[14] R.C. Agarwala, S. Ray, Z. Metallk. 83 (1992) 203–207.
[15] P.J. McGuiness, E.J. Devlin, M. Komelj, B. Podmiljsak, D. Niarchos, S. Kobe, J. Magn. Magn. Mater. 272–276 (2004) E1877–E1879.
[16] K.Z. Rozman, P.J. McGuiness, B. Podmiljsak, M. Rajic, S. Kobe, IEEE Trans. Magn. 40 (2004) 2952–2954.
[17] A. Hsiao, M.E. McHenry, D.E. Laughlin, M.J. Kramer, C. Ashe, T. Ohkubo, IEEE Trans. Magn. 38 (2002) 3039–3044.
[18] H.S. Ko, H.S. Park, K.T. Hong, K.S. Lee, M.J. Kaufman, Scr. Mater. 39 (1998) 1267–1272.
[19] L. Eleno, K. Frisk, A. Schneider, Intermetallics 14 (2006) 1276–1290.
[20] A.J. Bradley, J. Iron Steel Inst. 168 (1951) 233–244.
[21] G.W. Smith, Thermochim. Acta 291 (1997) 59–64.
[22] S. Divinski, Y.-S. Kang, W. Löser, C. Herzig, Intermetallics 12 (2004) 511–518.